ChemPubSoc Europe

DOI: 10.1002/cplu.201600477

CHEMPLUSCHEM Communications

# Crystal Engineering of a Two-Dimensional Lead-Free Perovskite with Functional Organic Cations by Second-Sphere Coordination

Daniele Cortecchia,[a, c] Cesare Soci,[b] Massimo Cametti,[d] Annamaria Petrozza,*[a] and Javier Martí-Rujas*[a]

Hybrid lead halide perovskite semiconductors are attracting increasing attention for applications in optoelectronics. However, the high lead content calls for the development of greener and smarter alternatives through crystal engineering. This is extremely challenging since the use of functional cations often results in the disruption of the metal halide framework. Here we show the rational design of a new lead-free, copper-based hybrid perovskite following a second-sphere coordination approach. Our synthetic strategy allows the incorporation of an organic cationic fluorophore within the two-dimensional Cu–Cl framework of a layered copper perovskite. The functionalization results in a moisture-stable and near-UV/blue-emitting copper perovskite. Along with the possibility of extending the emission in the visible range by further synthetic design, our approach paves the way for the development of a new class of Pb-free perovskites with potential applications in solid-state lighting.

Over the last four years, lead halide hybrid perovskites have been attracting major interest for applications in photovoltaic energy conversion,[1] photodetection and light emission.[2] In particular, light-emitting devices (LEDs),[3] field effect light-emitting transistors (LE-FETs)[4] and tunable lasers[5] were realized recently. Most of these technologies, however, rely heavily on Pb-based perovskites, such as methylammonium lead iodide ($MAPbI_3$) and cesium lead bromide ($CsPbBr_3$), and due to the toxicity and strict regulations of lead-based products[6,7] their commercialisation could be strongly hampered. For this reason the development of alternative lead-free perovskites is imperative.[8]

Copper-based layered perovskites, which are well known for their ferromagnetic properties,[9] have been recently studied for their piezochromism,[10] as lithium cycling material in hybrid electrodes[11] and as sensitizers in solar cells.[12] While these studies focused on transport and magnetic properties of the metal halide inorganic scaffold, inclusion of functional organic cations is also important in the design of new tailor-made smart functional materials.[13] In this regard, pioneering works have achieved efficient electroluminescence in two-dimensional (2D) lead perovskites combining the transport properties of the metal halide framework with the optical properties of an oligothiophene chromophore.[14,15] However, the use of bulky organic building blocks represents a big challenge as the steric hindrance is likely to disrupt the layered 2D structure of the metal halide networks, resulting in perovskite structures with different dimensionality, such as 1D or 0D.[16,17]

Crystal engineering principles aim at the rational design of solid materials by combining building blocks via self-recognition processes into new materials whose properties differ from those of the starting components. Up to a certain extent, crystal engineering allows the synthesis and the control of functional properties of solid materials such as porosity, magnetism and conductivity. The self-assembly of metal ions and organic cations via second-sphere coordination involving reversible hydrogen-bonding interactions can be used to design new materials with functional properties.[18] Second-sphere coordination, also known as outer-sphere coordination, refers to any intermolecular interaction with the ligands directly bound at the primary coordination sphere of a metal ion.[19] Hence, first-sphere ligands can form second-sphere adducts with virtually the whole range of noncovalent bonding interactions, such as coordination bonds, electrostatic, hydrogen bonding, halogen bonding, charge transfer and van der Waals interactions. In recent years, hybrid metal–organic materials self-assembled via second-sphere coordination have shown potential applications in gas adsorption,[20,21] separation[22] and nonlinear optical properties.[23]

In this study, we apply crystal engineering through second-sphere coordination interactions using charge-assisted hydrogen bonds to synthesise a new type of moisture-resistant "green" copper-based hybrid metal–organic perovskite that incorporates an optoelectronically active organic cation. The so-

[a] D. Cortecchia, Dr. A. Petrozza, Dr. J. Martí-Rujas
Istituto Italiano de Tecnologia Centre for Nano Science and Technology (CNST@PoliMi)
Politecnico di Milano
Via Pascoli 70/3, 20133 Milan (Italy)
E-mail: annamaria.petrozza@iit.it
javier.rujas@iit.it

[b] Prof. Dr. C. Soci
Division of Physics and Applied Physics
School of Physical and Mathematical Sciences
Nanyang Technological University, 637371 Singapore (Singapore)

[c] D. Cortecchia
Interdisciplinary Graduate School, Energy Research Institute (ERI@N)
Nanyang Technological University
Research Technoplaza, Nanyang Drive, 639798, Singapore (Singapore)

[d] Prof. Dr. M. Cametti
Dipartimento di Chimica Materiali
e Ingegneria Chimica „Giulio Natta"
Politecnico di Milano, Via Mancinelli 7, 20131 Milan (Italy)

Supporting information for this article can be found under http://dx.doi.org/10.1002/cplu.201600477.

lution-based synthesis is straightforward and can be carried out in a short time. As opposed to standard perovskites, where the cation has merely a structural function, the crystal engineering strategy applied here allows incorporation of a functional cation within the perovskite scaffold, conferring UV/blue photoluminescence (PL) and improved moisture stability. Since the synthetic design of the organic cation is flexible, the new material is an ideal platform to achieve optical properties on demand and has great potential as an alternative lead-free perovskite for light-emitting applications.

Instead of using 4,4′-bipyridine, which is known to form a similar type of 2D perovskite-like structures,[24] we chose here the organic building block 4,4′-(1,1′-biphenyl-4,4′-diyldioxy)dianiline (L). This ligand, which has a rigid rodlike geometry (ca. 19 Å length), can be considered to be composed of a conjugated oligoaromatic core (the biphenyl group) linked to two aniline anchoring units (Figure 1 a). These end groups make the

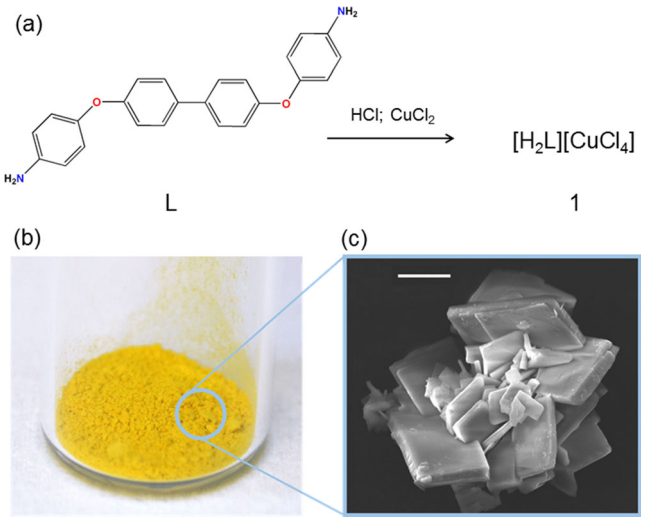


**Figure 1.** a) Synthesis of the 2D perovskite using the organic building block **L** and $CuCl_2$. b) Photograph of perovskite **1** yellow powder and b) SEM picture of a cluster of perovskite microcrystals showing the platelike crystal shape (scale bar = 5 μm).

ligand ditopic and increase its hydrophobicity since the aromatic units balance the hydrophilicity of the amino groups. In addition, the ether bridges and the biphenyl core contribute to the torsional flexibility of the bulky ligand which is accommodated in the final perovskite and stabilises the layered structure. The single-crystal X-ray (SC-XRD) structure of L shows the predisposition of the ligand in the crystal packing in terms of both C–H···π and π···π stacking interactions, and the hydrophilicity endowed by the amino groups which coordinate water molecules in the hydrated structure (Figure S1 in the Supporting Information).

When the preformed organic salt $[H_2L]Cl_2$[25] (Figure S2) was reacted with $CuCl_2$ in acidic (i.e., HCl) DMSO solution under ambient atmosphere, a fine yellow powder was instantly obtained (Figure 1 a, b). Scanning electron microscopy (SEM) images show that microcrystals with a platelike shape formed (Figure 1 c). Single crystals of micrometric size were structurally characterized by single-crystal X-ray diffraction (SC-XRD), confirming the formation of the hybrid 2D perovskite with formula $[H_2L][CuCl_4]$ (**1**).

In the structure, in the asymmetric unit there is half cation and half $[CuCl_4]^{2-}$ anion, and there is no solvent included. The two amine groups in the organic cation are protonated and act as hydrogen-bond donors. By means of second-sphere coordination interactions, the organic ammonium groups interact with the $[CuCl_4]^{2-}$ metal ion via three N–$H^+$···$Cl^-$ charge-assisted hydrogen bonds with N–Cl distances ranging from 3.174 Å to 3.282 Å and N–$H^+$···$Cl^-$ angles going from 145° to 169°, forming a well-defined organic layer (Figure 2 a). The molecular packing in the hybrid material induces a nearly perfect planar conformation of the biphenyl (torsion angle = 2.718°), which allows the maximum electronic delocalization between the adjacent aromatic rings.[26]

Regarding the inorganic part of the structure, $[CuCl_4]^{2-}$ units are arranged by alternating Cu···Cl–Cu bridges which ultimately forms an infinite 2D layer extending along the *bc* plane where each $Cu^{II}$ center adopts an octahedral coordination geometry, distorted by an evident Jahn–Teller effect. In fact, the Cu–Cl1 distances are 2.284 Å, 2.283 Å and 2.293 Å, while the longest one is the Cu–Cl2, 2.884 Å. The two longest distances correspond to the chloride-bridged Cl-$\mu$-Cl bond. An important aspect is that the 2D perovskite can also be prepared as powders homogeneously. The X-ray powder diffraction pattern of the bulk powder is the same as that simulated from single-crystal X-ray data indicating that the powder material has the same structure as the single crystal (Figure S3 a).

Interestingly, the N–$H^+$···$Cl^-$ charge-assisted hydrogen bonds are strong enough to overcome the hydrogen bonding with water molecules (observed in the free ligand L, Figure S1) yielding a completely water-free material. The second-sphere interactions, together with the aromatic character of the ligand, contribute to strongly protect the final material against moisture, which is generally detrimental for the stability of the hybrid perovskite.[27] Moreover, as observed in other isostructural Pb-based compounds, the intrinsic layered structure of the 2D perovskite contributes to further obstruct water diffusion in the material as compared to the standard 3D perovskites.[28] Indeed, this was confirmed by exposing the perovskite powders to air for one month, which did not cause significant changes in the powder X-ray diffraction pattern of the material (Figure S3).

The observed octahedral distortion is in agreement with the $Cu^{2+}$ electronic configuration $3d^9$ ($t_{2g}^6 g^3$), which is particularly prone to undergo Jahn–Teller distortion in an octahedral crystal field. The coordination complex $[CuCl_6]^{4-}$, with distorted octahedral coordination, is therefore characterized by a series of d–d transitions based on $Cu^{2+}$ (Figure 3 a,), giving rise to a broad absorption band in the near-infrared region (NIR) between 8000–1600 $cm^{-1}$ (625–1250 nm; Figure 3 b).

Analysis of this broad band by principal-component fitting yields the contributions of three components. These bands, peaking at 10893 $cm^{-1}$, 12281 $cm^{-1}$ and 13286 $cm^{-1}$ are assigned to the electronic transitions Cu $d_{xz,\,yz} \rightarrow$ Cu $d_{x^2-y^2}$,

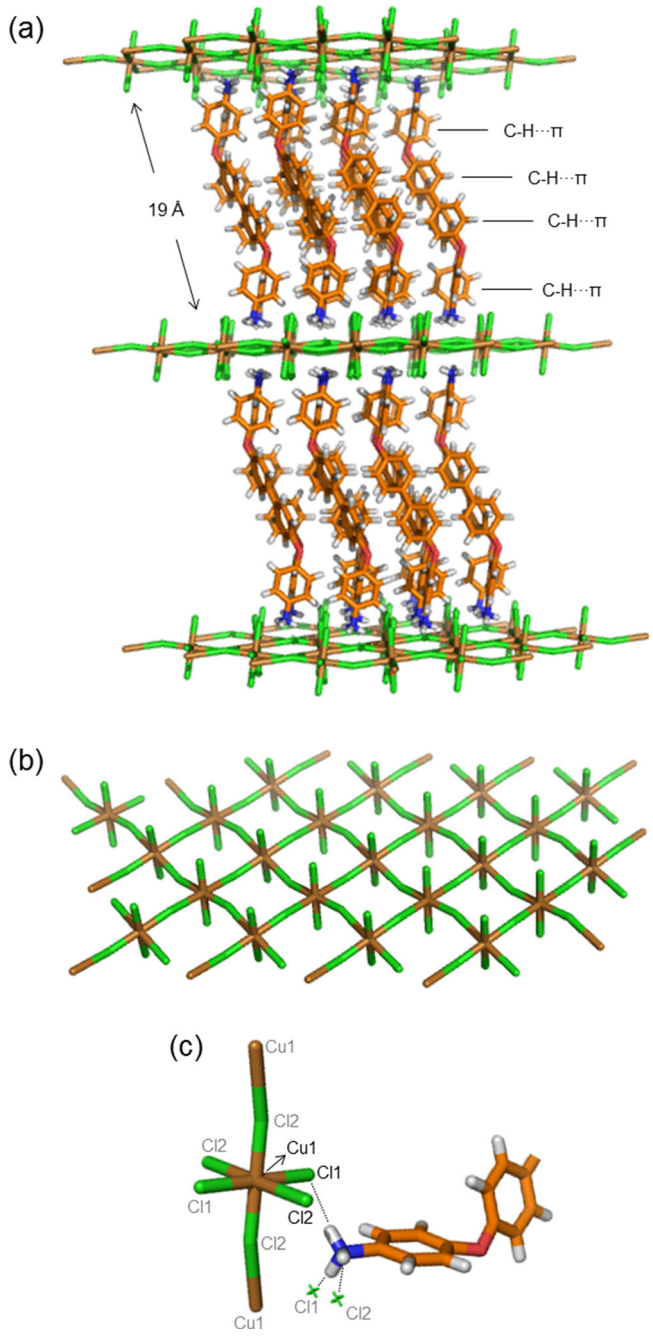


**Figure 2.** a) Crystal structure of the 2D hybrid perovskite **1** showing the layered nature. b) Enlarged view of the layered nature of the inorganic part of the second-sphere adduct. c) Detailed view of part of the structure of **1** showing the second-sphere charge-assisted hydrogen-bonding interactions (shown as black dashed lines9 established among the $NH_3^+$ groups and the chloride ligands in the first sphere. Colour code: carbon (orange); oxygen (red); nitrogen (blue); copper (brown); chloride (green); hydrogen (white).

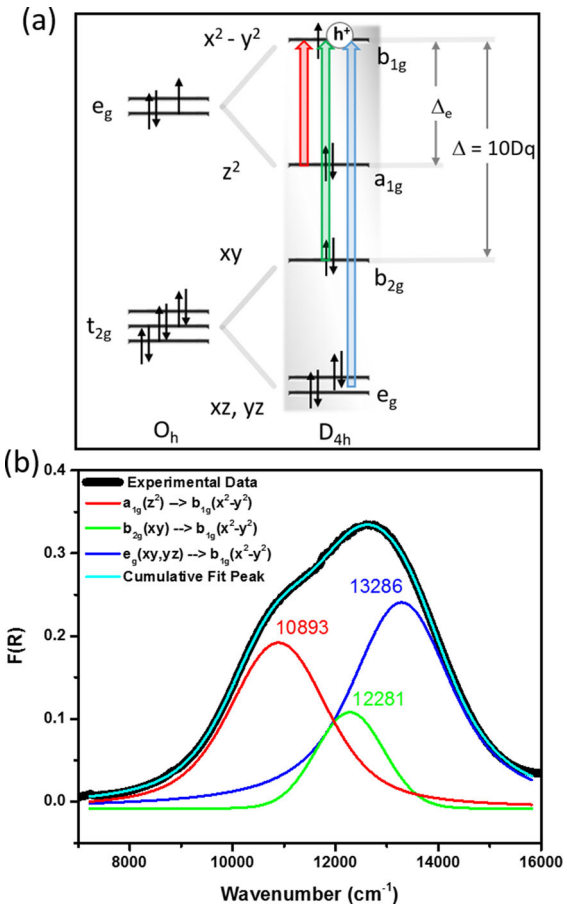


**Figure 3.** Optical characterization of **1** in the NIR region. a) Schematic energy diagram for a distorted octahedral coordination (*D4h* symmetry) and corresponding allowed electronic transitions. b) Details of d–d transitions in the range 8000–1600 $cm^{-1}$ (625–1250 nm) and principle-component fitting showing the three electronic transitions contributing to the broadband NIR absorption in **1**.

Cu $d_{xy}$ →Cu $d_{x^2-y^2}$, and Cu $d_{z^2}$ →Cu $d_{x^2-y^2}$,[12,29] respectively, in agreement with the orbital energy levels of a $d^9$ configuration in octahedral field (Oh) and *z*-out distortion ($D_{4h}$) (Figure 3a). Accordingly, the coordination complex $[CuCl_6]^{4-}$ shows a splitting of the $e_g$ levels $\Delta_e = 10\,893\ cm^{-1}$, $10Dq = 12\,281\ cm^{-1}$ and crystal field stabilization energy CFSE = 0.6 × 10*Dq* = 88.1 kJ $mol^{-1}$, which is in agreement with the values previously reported for similar hybrid copper perovskites.[10,29]

The presence of the optoelectronically active building block $H_2L^{2+}$ in the structure of the 2D perovskite prompted us to study the photoluminescence properties of **1**. Figure 4a shows the transformed Kubelka–Munk function *F*(*R*) obtained from the powder reflectance *R* according to the equation $F(R) = (R-1)^2/2R$ (Figure S4, Supporting Information), which gives a spectrum proportional to the absorption coefficient of the material. The spectrum of the 2D perovskite **1** features two main absorption bands: one below 350 nm and a second peaking at 380 nm, with a shoulder at 440 nm. The latter, with a direct bandgap of 464 nm (2.67 eV, Figure S4d, Supporting Information) can be attributed to ligand-to-metal charge-transfer (CT) transitions, in agreement with similar copper perovskites.[12,30,31] Such CT states occur between the first-sphere coordination ligands (Cl) and the highest antibonding of the d orbitals based on copper, and can be expressed as Cl pσ→ Cu $d_{x^2-y^2}$ and Cl pπ→Cu $d_{x^2-y^2}$. Conversely, the higher energy band fits well the absorption of $[H_2L]Cl_2$, with a band gap of 326 nm (3.80 eV, Figure 4a and Figure S4b, Supporting Infor-

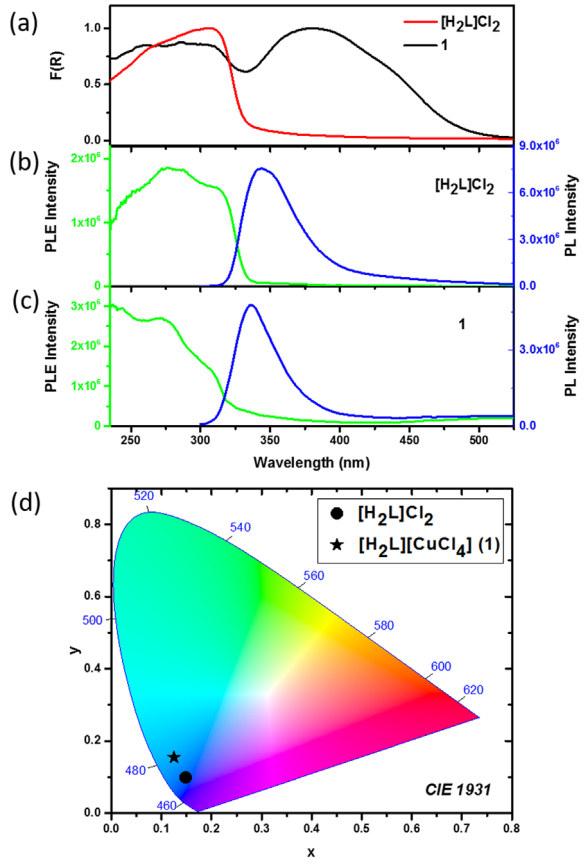


**Figure 4.** a) Transformed powder reflectance spectrum of the organic salt precursor $[H_2L]Cl_2$ (red) and **1** (black). Photoluminescence properties of b) $[H_2L]Cl_2$ and c) **1**: photoluminescence (PL) spectrum at $\lambda_{exc} = 280$ nm (green) and photoluminescence excitation spectrum (PLE) at $\lambda_{probe} = 360$ nm (blue). d) Chromaticity coordinates (CIE 1931) of $[H_2L]Cl_2$ and **1**.

mation), and can be assigned to electronic transitions in the organic component.

Moreover, $[H_2L]Cl_2$ shows bright photoluminescence peaking at 343 nm, with full width at half maximum (FWHM) of 45 nm and a Stoke shift of 17 nm (Figure 4b), in good agreement with the fluorescence of biphenyl and biphenyl derivatives.[32,33,34,35] Interestingly, the photoluminescence properties of the organic ligand are retained upon self-assembly of the perovskite framework: at an excitation wavelength of 280 nm, the hybrid perovskite **1** shows fluorescence with $\lambda_{max} = 336$ nm (Figure 4c). This emission is largely blue-shifted compared to the perovskite CT transitions, and therefore cannot be associated to emission from the perovskite band-edge (464 nm).

On the other hand, the excitation spectrum ($\lambda_{em} = 360$ nm) of the perovskite (Figure 4c) perfectly matches the excitation spectrum of the organic salt $[H_2L]Cl_2$ as well as its absorption spectrum (Figure 4a, b), indicating the successful functionalization with the organic cation. The slight blue shift (7 nm) and narrowing (FWHM decrease of 9 nm) of the emission band in the perovskite may be attributed to the different packing of the $H_2L^{2+}$ cations in the constrained perovskite lattice. In fact, the molecular packing was found to vary in the three crystals based on the L ligand (Figure S4, Supporting Information). This involves slight differences in the torsion angle of the biphenyl (with consequent change in electronic delocalization) and modifications in the intermolecular forces holding the crystal (C–H···π and π···π stacking interactions), which are likely to affect the collective excited state of the resulting solid.

The emission spectra of both the materials contain a visible component giving a nearly pure blue colour with CIE coordinates (0.148; 0.099) for $[H_2L]Cl_2$ and (0.125; 0.155) for the perovskite **1** (Figure 4d and Figure S6). However, the main emission of the perovskite **1** falls in the UV-A range ($\lambda_{em} = 320$–400 nm), which is a challenging spectral region to cover with traditional semiconductors; this region is currently reached with AlGaN quantum wells ($\lambda_{em} < 365$ nm)[36] and nanostructured ZnO in the near-UV/blue region.[37] Ultraviolet LEDs are typically fabricated with these materials for applications in high-density information storage, chemical biological analysis, or combined with phosphor mixtures to generate white light with high CRI (colour rendering index) values suitable for indoor applications.[38,39,40] While the luminescence properties of **1** are potentially suitable for such a down-conversion approach, the possibility of selectively introducing the organic cation also allows the tuning of the optoelectronic properties of the hybrid material with the possibility to span across the visible spectrum, increasing its relevance for applications in solid-state lighting. For example, the biphenyl could be easily functionalized with nitro and sulfonate groups to modulate its luminescence, or the conjugation could be increased by including carbazole and anthracene derivatives, placing **1** as the first member of a big family of functional hybrid, lead-free perovskites.

In summary, we have shown the rational synthetic design of a new hybrid copper perovskite through a second-sphere coordination approach. The new layered material **1** is based on 4,4′-(1,1′-biphenyl-4,4′-diyldioxy)dianiline as an organic building block and combines for the first time a two-dimensional copper chloride framework with an optoelectronically active bulky cation, achieving near-UV/blue photoluminescence and moisture resistance in the resulting hybrid. This study paves the way for the development of a new class of lead-free hybrid perovskites incorporating functional cations and allowing the tuning of optical properties through synthetic design by exploitation of second-sphere coordination interactions. These characteristics make hybrid functional copper perovskites a valuable alternative to Pb-based perovskites, with great potential for applications in solid-state lighting.

## Experimental Section

Single-crystal X-ray diffraction experiments were carried out with a Bruker X8 Prospector APEX-II/CCD diffractometer equipped with a focusing mirror (Cu K$\alpha$ radiation, $\lambda = 1.54056$ Å).

Single-crystal XRD data for **L**: $C_{24}H_{20}N_2O_3$, $M_r = 384.42$, monoclinic, $P\bar{1}$, $a = 5.6806(6)$ Å, $b = 7.9232(8)$ Å, $c = 21.668(2)$ Å, $\alpha = 93.567(7)^\circ$, $\beta = 97.413(7)^\circ$, $\gamma = 90.187(7)^\circ$, $V = 965.16(17$ Å$^3$, $T = 296(2)$ K, $Z = 2$, $\rho_{calcd} = 1.323$ g cm$^{-3}$, 3331 reflections measured, 2542 independent reflections, 262 parameters, 0 restraints, $2.060^\circ < \theta < 66.367^\circ$, $R_1$ [$I > 2\sigma(I)$] = 0.0845 and $wR^2$ [$I > 2\sigma(I)$] = 0.2909.

Single-crystal XRD data for $[H_2L]Cl_2$: $C_{28}H_{34}Cl_2N_2S_2$, $M_r = 597.58$, triclinic, $P\bar{1}$, $a = 5.6713(5)$ Å, $b = 8.2899(7)$ Å, $c = 15.9733(14)$ Å, $\alpha = 85.385(7)^\circ$, $\beta = 81.832(7)^\circ$, $\gamma = 78.316(6)^\circ$, $V = 726.92(11)$ Å$^3$, $T = 150(2)$ K, $Z = 2$, $\rho_{calcd} = 1.365$ g cm$^{-3}$, 2459 reflections measured, 2107 independent reflections, 175 parameters, 0 restraints, $2.799^\circ < \theta < 66.017^\circ$, $R_1$ $[I > 2\sigma(I)] = 0.0354$ and $wR^2$ $[I > 2\sigma(I)] = 0.0935$.

Single-crystal XRD data for **1**: $C_{24}H_{22}Cl_4Cu_1N_2O_3$, $M_r = 575.78$, monoclinic, $P21/c$, $a = 23.499(4)$ Å, $b = 7.4335(12)$ Å, $c = 7.0455(10)$ Å, $\beta = 97.462(12)^\circ$, $V = 1220.28(34)$ Å$^3$, $T = 296(2)$ K, $Z = 4$, $\rho_{calcd} = 1.567$ g cm$^{-3}$, 2128 reflections measured, 1471 independent reflections, 152 parameters, 0 restraints, $6.249^\circ < \theta < 66.637^\circ$, $R_1$ $[I > 2\sigma(I)] = 0.0986$ and $wR^2$ $[I > 2\sigma(I)] = 0.2641$.

CCDC 1484918, 1484919, and 1484920 (for L, $[H_2L]Cl_2$, **1**) contain the supplementary crystallographic data for this paper. These data are provided free of charge by The Cambridge Crystallographic Data Centre. Supporting Information contains additional crystallographic data and photophysical characterization.

## *Acknowledgements*

This research was supported by the Istituto Italiano di Tecnologia and by the Ministry of Education (MOE2013-T2–044) and the National Research Foundation (NRF-CRP14–2014–03) of Singapore.

**Keywords:** hydrogen bonds · crystal engineering · metal–organic frameworks · perovskite phases · second-sphere coordination

[1] T. M. Brenner, D. A. Egger, L. Kronik, G. Hodes, D. Cahen, *Nat. Rev. Mater.* **2016**, *1*, 15007.
[2] S. D. Stranks, H. J. Snaith, *Nat. Nanotechnol.* **2015**, *10*, 391 – 402.
[3] H. Cho, S.-H. Jeong, M.-H. Park, Y.-H. Kim, C. Wolf, C.-L. Lee, J. H. Heo, A. Sadhanala, N. Myoung, S. Yoo, S. H. Im, R. H. Friend, T.-W. Lee, *Science* **2015**, *350*, 1222 – 1225.
[4] X. Y. Chin, D. Cortecchia, J. Yin, A. Bruno, C. Soci, *Nat. Commun.* **2015**, *6*, 7383 – 7892.
[5] F. Deschler, M. Price, S. Pathak, L. E. Klintberg, D. D. Jarausch, R. Higler, S. Hüttner, T. Leijtens, S. D. Stranks, H. J. Snaith, M. Atatüre, R. T. Phillips, R. H. Friend, *J. Phys. Chem. Lett.* **2014**, *5*, 1421 – 1426.
[6] Y. Li, K.-s. Moon, C. P. Wong, *Science* **2005**, *308*, 1419 – 1420.
[7] A. Babayigit, A. Ethirajan, M. Muller, B. Conings, *Nat. Mater.* **2016**, *15*, 247 – 251.
[8] a) F. Hao, C. C. Stoumpos, D. H. Cao, R. P. H. Chang, M. G. Kanatzidis, *Nat. Photonics* **2014**, *8*, 489 – 594; b) A. H. Slavney, R. W. Smaha, I. C. Smith, A. Jaffe, D. Umeyama, H. I. Karunadasa, *Inorg. Chem.* **2016**, *55*, 10.1021/acs.inorgchem.6b01336.
[9] R. Willett, H. Place, M. Middleton, *J. Am. Chem. Soc.* **1988**, *110*, 8639 – 8650.
[10] A. Jaffe, Y. Lin, W. L. Mao, H. I. Karunadasa, *J. Am. Chem. Soc.* **2015**, *137*, 1673 – 1678.
[11] A. Jaffe, H. I. Karunadasa, *Inorg. Chem.* **2014**, *53*, 6494 – 6496.
[12] D. Cortecchia, H. A. Dewi, J. Yin, A. Bruno, S. Chen, T. Baikie, P. P. Boix, M. Grätzel, S. Mhaisalkar, C. Soci, N. Mathews, *Inorg. Chem.* **2016**, *55*, 1044 – 1052.
[13] B. Saparov, D. B. Mitzi, *Chem. Rev.* **2016**, *116*, 4558 – 4596.
[14] K. Chondroudis, D. B. Mitzi, *Chem. Mater.* **1999**, *11*, 3028.
[15] D. B. Mitzi, K. Chondroudis, C. R. Kagan, *Inorg. Chem.* **1999**, *38*, 6246 – 6256.
[16] G. Kieslich, S. Sun, A. K. Cheetham, *Chem. Sci.* **2015**, *6*, 3430.
[17] A. E. Maughan, J. A. Kurzman, J. R. Neilson, *Inorg. Chem.* **2015**, *54*, 370 – 378.
[18] a) F. Guo, H. D. Shao, Q. Yang, A. Famulari, J. Martí-Rujas, *CrystEngComm* **2014**, *16*, 969 – 973; b) H. Y. Guan, Z. Wang, A. Famulari, X. Wang, F. Guo, J. Martí-Rujas, *Inorg. Chem.* **2014**, *53*, 7438 – 7445; c) F. Guo, J. Martí-Rujas, *Dalton Trans.* **2016**, *45*, 13648 – 13662.
[19] a) S. J. Loeb in *Comprehensive Supramolecular Chemistry, Vol. 1* (Eds.: J. L. Atwood, J. E. D. Davies, D. D. MacNicol, F. Vögtle), Elsevier Science New York **1996**, p. 733; b) Z. Liu, S. T. Schneebeli, J. F. Stoddart, *Chimia* **2014**, *68*, 315 – 320.
[20] S. A. Dalrymple, G. K. H. Shimizu, *J. Am. Chem. Soc.* **2007**, *129*, 12114 – 12116.
[21] N. Roques, G. Mouchaham, C. Duhayon, S. Brandes, A. Tachon, G. Weber, J. P. Bellat, J.-P. Sutter, *Chem. Eur. J.* **2014**, *20*, 11690 – 11694.
[22] a) Z. Liu, M. Frasconi, J. Lei, Z. J. Brown, Z. Zhu, D. Cao, J. Iehl, G. Liu, A. C. Fahrenbach, Y. Y. Botros, O. K. Farha, J. T. Hupp, C. A. Mirkin, J. F. Stoddart, *Nat. Commun.* **2013**, *4*, 1855; b) Z. Liu, A. Samanta, J. Lei, J. Sun, Y. Wang, J. F. Stoddart, *J. Am. Chem. Soc.* **2016**, *138*, 11643 – 11653.
[23] H. B. Yu, H. T. Li, P. Zhang, A. Famulari, F. Guo, I. Bargigia, J. Martí-Rujas, *CrystEngComm* **2016**, *18*, 2408 – 2412.
[24] B. Dolling, A. L. Gillon, A. G. Orpen, J. Starbuck, X. M. Wang, *Chem. Commun.* **2001**, 567 – 568.
[25] The crystal structure of the chloride salt was determined by single crystal and powder X-ray analysis. See the Supporting Information for further information.
[26] T. A. Su, M. Neupane, M. L. Steigerwald, L. Venkataraman, C. Nuckolls, *Nat. Rev. Mater.* **2016**, *1*, 16002.
[27] A. Leguy, Y. Hu, M. Campoy-Quiles, M. I. Alonso, O. J. Weber, P. Azarhoosh, M. van Schilfgaarde, M. T. Weller, T. Bein, J. Nelson, P. Docampo, P. R. F. Barnes, *Chem. Mater.* **2015**, *27*, 3397 – 3407.
[28] I. C. Smith, E. T. Hoke, D. Solis-Ibarra, M. D. McGehee, H. I. Karunadasa, *Angew. Chem. Int. Ed.* **2014**, *53*, 11232 – 11235; *Angew. Chem.* **2014**, *126*, 11414 – 11417.
[29] R. D. Willett, O. L. Liles, C. Michelson, *Inorg. Chem.* **1967**, *6*, 1885 – 1889.
[30] S. R. Desjardins, K. W. Penfield, S. L. Cohen, R. L. Musselman, E. I. Solomon, *J. Am. Chem. Soc.* **1983**, *105*, 4590 – 4603.
[31] S. Gupta, T. Pandey, A. K. Singh, *Inorg. Chem.* **2016**, *55*, 6817 – 6824.
[32] E. Abuin, E. Lissi, L. Gargallo, D. Radic, *Eur. Polym. J.* **1982**, *18*, 319.
[33] S. Chen, N. E. Fahmi, C. Bhattacharya, L. Wang, Y. Jin, S. J. Benkovic, S. M. Hecht, *Biochemistry* **2013**, *52*, 8580 – 8589.
[34] H. Du, R.-C. A. Fuh, J. Li, L. A. Corkan, J. S. Lindsey, *Photochem. Photobiol.* **1998**, *68*, 141 – 142.
[35] V. I. Levshin, K. I. Mamedov, S. R. Sergienko, S. D. Pustil'nikova, *Bull. Acad. Sci. USSR Div. Chem. Sci. (Engl. Transl.)* **1959**, *8*, 1514.
[36] A. Khan, K. Balakrishnan, T. Katona, *Nat. Photonics* **2008**, *2*, 77 – 84.
[37] J. H. Lim, C. K. Kang, K. K. Kim, I. K. Park, D. K. Hwang, S. J. Park, *Adv. Mater.* **2006**, *18*, 2720 – 2724.
[38] E. F. Schubert, J. K. Kim, *Science* **2005**, *308*, 1274 – 1278.
[39] M. H. Crawford, *IEEE J. Sel. Top. Quantum Electron.* **2009**, *15*, 1028 – 1040.
[40] S. Pimputkar, J. S. Speck, S. P. DenBaars, S. Nakamura, *Nat. Photonics Nat.* **2009**, *3*, 180 – 182.

Manuscript received: September 19, 2016
Accepted Article published: October 24, 2016
Final Article published: ■■ ▮▮, 0000

# COMMUNICATIONS

*D. Cortecchia, C. Soci, M. Cametti, A. Petrozza,* J. Martí-Rujas**

■■ – ■■

**Crystal Engineering of a Two-Dimensional Lead-Free Perovskite with Functional Organic Cations by Second-Sphere Coordination**

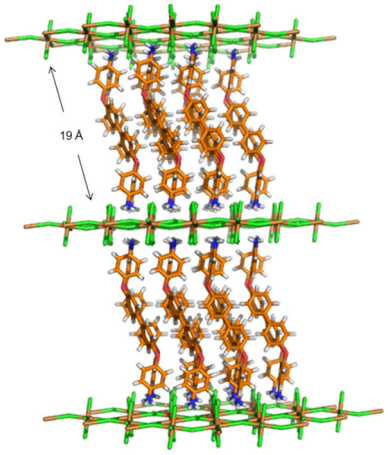


**Functional cations**: A new two-dimensional Cu perovskite containing an optoelectronically active organic cation (orange in the figure) has been synthesized using second-sphere coordination interactions. The material shows near-UV/blue photoluminescence and is stable for months under ambient conditions.